Failure Load Prediction and Optimisation for Adhesively Bonded Joints Enabled by Deep Learning and Fruit Fly Optimisation

Weidong Li[1], Yuchen Liang[2]†, Yiding Liu[3]

[1] School of Mechanical Engineering, University of Shanghai for Science and Technology, China

[2] College of Engineering, Coventry University, Coventry, U.K.

[3] School of Physics, Engineering & Computer Science, University of Hertfordshire, U.K.

† Corresponding author: ad2586@coventry.ac.uk

Abstract

Adhesively bonded joints have been extensively employed in the aeronautical and automotive industries to join thin-layer materials for developing lightweight components. To strengthen the structural integrity of joints, it is critical to estimate and improve joint failure loads effectually. To accomplish the aforementioned purpose, this paper presents a novel deep neural network (DNN) model-enabled approach, and a single lap joint (SLJ) design is used to support research development and validation. The approach is innovative in the following aspects: (i) the DNN model is reinforced with a transfer learning (TL) mechanism to realise an adaptive prediction on a new SLJ design, and the requirement to re-create new training samples and re-train the DNN model from scratch for the design can be alleviated; (ii) a fruit fly optimisation (FFO) algorithm featured with the parallel computing capability is incorporated into the approach to efficiently optimise joint parameters based on joint failure load predictions. Case studies were developed to validate the effectiveness of the approach. Experimental results demonstrate that, with this approach, the number of datasets and the computational time required to re-train the DNN model for a new SLJ design were significantly reduced by 92.00% and 99.57% respectively, and the joint failure load was substantially increased by 9.96%.

Keywords: Adhesively bonded joint, Deep neural network, Transfer learning

1. Introduction

Adhesively bonded joints have been widely used to attach thin-layer materials together to develop structural components for fulfilling versatile functions in aerospace, automotive, civil engineering, etc. The joints possess some distinguishing advantages over traditional joints, such as weight reduction, stress concentration minimisation along joint overlapping lengths, good manufacturability, and bondability of similar/dissimilar materials (Kim et al., 2021). According to the summary of the adhesively bonded joint technology (Sadeghi et al., 2020), some widely-adopted forms include single lap joints, double lap joints, scarf joints, single L-shape joints, and single T-shape joints (some of them are illustrated in Fig. 1). Owing to the relatively simpler geometrical configuration and manufacturing process, the single lap joint (SLJ) is one of the most typical forms and it has been extensively adopted in various industrial applications (Djebbar et al., 2022). In this paper, SLJs are used to exemplify the research innovations in predicting and optimising adhesively bonded joints.

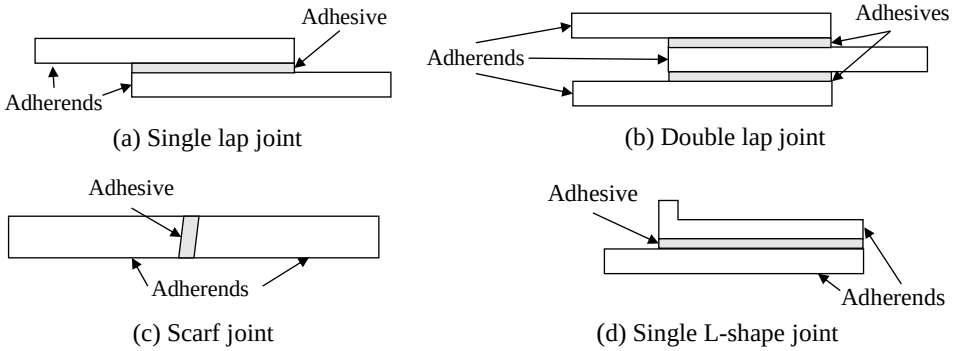

Fig. 1: Several typical configurations of adhesively bonded joints.

It is a paramount research topic to strengthen the structural integrity of adhesively bonded joints. An integral joint should exhibit good shear properties, generate uniform stress distributions upon loading, hold high fatigue resistance and impermeability, and have good compatibility properties with a wide range of different dissimilar materials (Shi et al., 2019; Demir et al., 2020; Gavgali et al., 2021). When a tensile load is applied to an SLJ, a bending moment will be created, causing peeling stress on the edges of the overlapping regions in the joint (Demir et al., 2020). During this process, the joint failure load is a critical factor reflecting

the integrity and performance of bonded structures (Akpinar and Sahin, 2021; Abdel-Monsef et al., 2021). The joint failure load is correlated with various variables, such as type, size, alkaline treatment, weight ratio, elastic modulus and fracture toughness of adherends and adhesives (Liu et al., 2021). Usually, the value of the joint failure load is acquired through lap shear tests on bundles of joint coupons. Physical tests, however, are expensive in setup or even impractical to be carried out for every category of adherends and adhesives. To minimise the number of required tests and associated costs, finite element analysis (FEA) models have been adopted (Kupski and Teixeira de Freitas, 2021). Based on FEA models, bonding conditions and failure loads of adhesively bonded joints in complex geometrical shapes and joining configurations can be assessed more conveniently in comparison with physical tests. For FEA-models, just a small number of physical tests will be required to calibrate the established FEA models so that the total number of tests would be diminished to a great extent. Nevertheless, FEA modelling is highly expertise-dependent, and therefore it is not an ideal solution for industries, especially small and medium-sized enterprises, to adopt. Moreover, FEA modelling is computationally intensive, making the optimisation process of a new joint design inefficient. The reason is that a large number of iterative FEA-based simulations will take place.

Recently, deep learning algorithms have been actively investigated to develop effective assessment or prediction models in supporting various applications. One significant characteristic of deep learning algorithms is that features and their underlying correlations can be mined from a large amount of data intelligently and autonomously. The algorithms, once trained, can be used in applications as a black-box decision-making tool and therefore, the expertise of engineering physics is less required. Owing to this distinguishing advantage, deep learning algorithms have demonstrated great potential to facilitate the estimation and optimisation of joint failure loads. Nevertheless, relevant research has not been actively carried out yet.

Based on the strength of deep learning algorithms, in this research, a deep neural network (DNN) model-enabled approach is devised to efficiently predict the failure loads of SLJs and optimise the joint design. Firstly, the DNN model is initially trained using datasets generated

by FEA modelling and calibrated by a small number of critical physical tests. Secondly, for new SLJs with different materials and parameters, the DNN model is reinforced with a transfer learning (TL) mechanism to realise adaptive predictions on the new designs. In this way, the expertise required in FEA modelling for new SLJ designs can be greatly alleviated. Finally, a fruit fly optimisation (FFO) algorithm is embedded in the approach to iteratively fine-tune key joint parameters for optimised joint design based on predictions on joint failure loads. In this research, case studies were introduced to justify the effectiveness and robustness of the approach. Experimental results showed that, in comparison with FEA modelling, the number of datasets and computational time required for re-training the DNN model for a new SLJ design were diminished by 92.00% and 99.57%, respectively. The case study also demonstrated that, with optimised parameters achieved by the FFO algorithm, the joint failure load was upscaled by 9.96%. Furthermore, in this research, optimal configurations of the approach were pinpointed through benchmarking analyses, and the effectiveness and superiority of the FFO algorithm over some mainstream algorithms were evidenced based on comparative results.

The rest of this paper is organised as follows. In Section 2, related research is summarised, and research gaps arising from the survey are identified. In Section 3, the developed approach is detailed from the perspectives of methodology framework, experimental setup, FEA modelling, improved DNN modelling with the TL mechanism, and the FFO algorithm design. In Section 4, case study results and comparisons of the approach are presented, visualised and analysed. In Section 5, conclusions are drawn and future research directions are outlined.

2. Review on Related Work

Research work for modelling and analysing the joint failure loads of adhesively bonded joints has been steadily carried out. Several survey papers were published to update the relevant progress (Shang et al., 2019; Ramalho et al., 2020a, 2020b). The surveys reported that mainstream analytical methods include the Ojalvo–Eidinoff model (Ojalvo and Eidinoff, 1978), the Volkersen's model (Carbas et al., 2014), the Goland-Reissner model (Stein et al., 2016a), the Shear-Lag model (Stein et al., 2016b), etc. These models usually only require the acquisition

of stress/strain values from the adhesive layer of a joint to estimate its failure load. Nevertheless, when the geometries and configurations of joints are intricate, these analytic models are less accurate and ineffective. To tackle the issue, in recent years, FEA-based analytic and prediction models have been developed. Matta and Ramji (2019) developed a 2D FEA model to estimate the mechanical behaviour of an adhesive bonded joint under the tensile load. FEA simulation results, including the initial stiffness, failure load and displacement, were compared with experimental results to ensure the validity of the FEA model. Jairaja and Naik (2019) analysed the bonding stress and failure patterns of both single and dual adhesively bonded joints using FEA models and experimental models. FEA-based simulations proved that the design of the dual joint increased the failure loads of joints. Ye et al. (2019) designed an improved 3D coupled exponential cohesive zone model enabled by an FEA model to analyse the tensile failure load of an adhesively bonded joint. The FEA model was justified by experimental data, and the influence of joint parameters such as overlapping lengths on the joint failure load was analysed. Behera et al. (2020) examined the critical damage location of an adhesively bonded joint. It proved that the variations of peeling stress and shear stress in the overlapping regions of a joint were complicated, so an FEA model was a preferable tool used to visualise the stress distribution. Dehaghani et al. (2021) developed a 3D FEA model to envisage the failure load of SLJs. The model was used to guide an optimal surface treatment process to maximise the failure load of a joint to meet the requirements of engineering applications.

In recent years, machine learning (including deep learning) technologies have been leveraged to model and predict the failure loads of adhesively bonded joints to better facilitate joint design optimisation. Once well-trained offline, a machine learning algorithm will perform online prediction much faster than FEA-based simulations, and the expensive setups for laboratory experiments are not necessary. Atta et al. (2019) adopted FEA and artificial neural networks (ANNs) to assess the failure stages of double lap bolted joints. Training samples for the ANNs were generated from the FEA model, so that the cost to set up and conduct laboratory experiments was greatly minimised. Wang et al. (2021) designed ANNs-driven prediction models to estimate the curved cracks of joints under variable amplitude loads. However, the

proposed ANNs models were unable to achieve enough prediction accuracy. Gu et al. (2021) developed a deep learning model to predict the failure load of an SLJ. The model was trained based on 300 data samples produced by an FEA model and validated with experimental data. The issue in this research is that the trained DNN model was rigid and only applicable to the designed SLJ with specific parameters. It is inappropriate to support joint optimisation design as the parameters of the joint need to be fine-tuned iteratively.

To optimise the design of adhesively bonded joints, optimisation algorithms were developed to identify the best parameters for the joints. Barzegar et al. (2021) designed three optimisation algorithms, i.e., SGDM (the stochastic gradient descent with momentum), SVRG (the stochastic variance-reduced gradient), and FISTA (the fast iterative shrinkage-thresholding algorithm), to identify the optimal parameters of adhesively bonded aluminium joints. However, it was challenging to determine suitable initial parameters in the algorithms (e.g., learning rate and weighting parameters). Arhore et al. (2021) developed two optimisation algorithms, i.e., the genetic algorithm (GA)-based optimisation and the topology optimisation (TOP), to resolve this problem. Results showed that TOP can find the joint failure load in a more robust means, and the GA algorithms can identify an optimal strength-to-weight ratio of the joint. Nevertheless, there is still no research reported to integrate the failure load prediction and parameter optimisation of adhesively bonded joints to effectively improve the joint design.

In summary, research gaps arising from the aforementioned survey are identified below:

- Existing works based on FEA-enabled prediction models are hindered by the challenging issues of expertise dependency and heavy computational workloads. It means that a designed FEA model is only applicable to a specific joint design, instead of multiple ones with different joint parameters. It is imperative to develop more versatile models that are adaptive to various joint designs in an efficient means;
- Existing works based on machine learning-enabled models can accelerate the efficiency of online predictions significantly. However, the models are less adaptive in supporting new joint designs, and it is inevitable to re-collect and re-train for the new design;

- It is desirable to develop a systematic process of integrating a machine learning algorithm and a robust metaheuristic optimisation algorithm to provide effectual prediction and optimisation functions to improve new joint designs.

3. Research Methodology

3.1 The overall procedure of the approach

This paper presents a novel approach to address the aforementioned research gaps. The functions and information flow of the approach, which are illustrated in Fig. 2, are described below. More technical details are further elaborated on and discussed in later sub-sections.

(i) FEA modelling for training sample generation and validation via critical physical tests: A FEA model is developed to simulate aluminium alloy SLJs bonded with epoxy adhesives. The inputs to the model are several key joint parameters, including E_1 (the elastic modulus of the upper adherend), E_2 (the elastic modulus of the lower adherend), G_1 (Mode I fracture toughness of the adhesive), and G_2 (Mode II fracture toughness of the adhesive). Lap shear tests for the joints are set up, and joint load-displacement data are collected via the experiments. The experiments are used to calibrate the training samples from the FEA model. During the above experimental procedures, G_1 and G_2 are measured from the mode I double cantilever beam (DCB) and the mode II end notch flexure (ENF) standard tests according to the ISO 15024 standard (2001) and ASTM D6671 (2006). For SLJs, prediction of the lap shear strength depends on the accuracy of the measured G_1 and G_2;

(ii) Design of the DNN model to be trained using the above simulation datasets: Different DNN structures and hyperparameters are compared and analysed to determine an optimal DNN model. Datasets generated by the above FEA model are employed for the DNN model training. The optimal number of FEA datasets is evaluated to identify the best computational accuracy and efficiency of the DNN model;

(iii) Design of the TL mechanism to optimise the re-training process of the DNN model: When joint parameters are changed to be a new joint design, only a small number of new

datasets need to be generated via experiments and FEA simulation to calibrate the DNN model based on the TL mechanism embedded in the DNN model;

(iv) Design of the FFO algorithm to pursue the best joint parameters: Based on the predictive model, the FFO algorithm is designed and conducted to pinpoint optimal joint parameters to extend the joint failure load. The DNN model will generate the joint failure loads of an adhesively bonded joint in different parameters (E_1, E_2, G_1, G_2) to support joint optimisation enabled by the FFO algorithm.

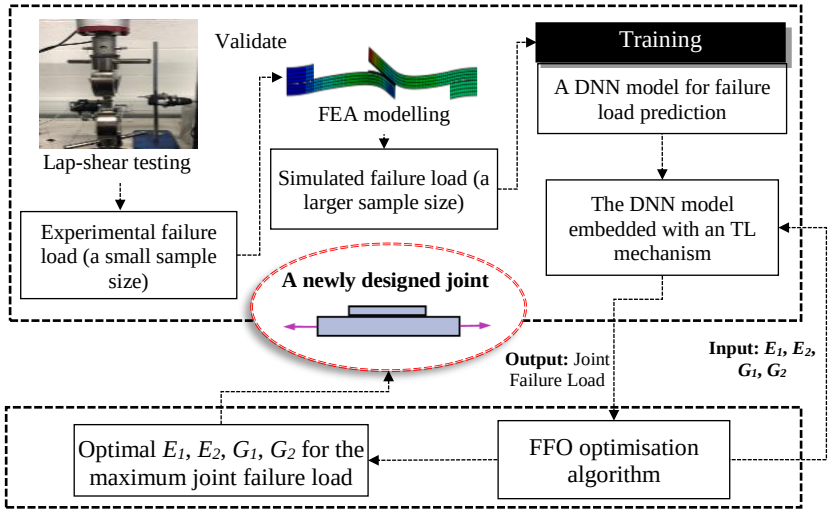

Fig. 2: The overall framework of the research methodology.

3.2 Experimental setup

The specifications of joint coupons in the experiment to support the approach are described below. Aluminium and composite SLJs, which were designed according to the ASTM D3165 standard (2014) (ASTM D3165, 2014), were tested for research methodology development and validation. The technical details of the two joints are given in Fig. 3. For the aluminium and composite joints, the adherends were manufactured from the aluminium alloy 6110-T6 and the woven Carbon Fibre Reinforced Plastic (CFRP), respectively. The adhesive used for both joints is Araldite® 2015.

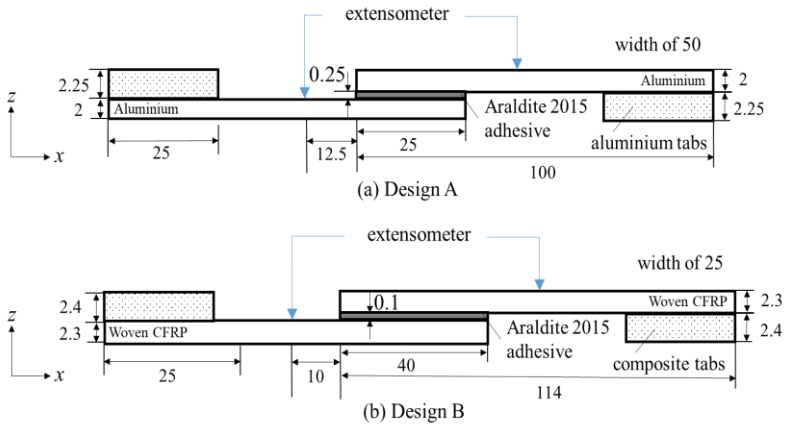

Fig. 3: Two SLJ designs adopted from the ASTM D3165 standard (unit in mm).

For the aluminium SLJ, the nominal thicknesses of the adherends and the adhesive are 2.00 mm and 0.25 mm, respectively. The surfaces of adherends were treated by abrasive sanding using a P40 sandpaper followed by a cleaning process with an ethanol solvent. A thin layer of the Sika Primer 204N was applied to favour the chemical bond at the adherend-adhesive interface. For the composite joint, the nominal thicknesses of the adherends and the adhesive were 2.30 mm and 0.10 mm, respectively. A coupled surface treatment was conducted by using grit blasting (Guyson Grade 13) followed by a cleaning process with a Propan-2-ol solvent to improve the bonding quality. The thickness of the adhesive was controlled using glass beads in a given diameter for both cases. The joint specimens were cured at 120 ºC for 40 minutes by using a clamping jig with fasteners to ensure a uniform adhesive layer. Aluminium-based end tabs were prepared to reduce the bending moment and avoid damage to the adherends during the experimental tests. The material properties of both adherends and adhesive, and cohesive parameters of the adhesive are given in Table 1.

Table 1: Properties of the adherends and adhesives (Huntsman, 2015).

Property	**Aluminium**	**Woven CFRP**	**Araldite® 2015**
Young's modulus, E (GPa)	70.00	E_1=76.39, E_2=69.69	1.85 ± 0.21
Poisson ratio, v	0.30	v_{12}= v_{21}=0.51	0.33
Tensile failure strength, σ_f (MPa)	Not required		21.63 ± 1.61
Shear failure strength, τ_f (MPa)			17.90 ± 1.80
Toughness in tension, G_n^c (N/mm)			0.43 ± 0.02
Toughness in shear, G_s^c (N/mm)			4.70 ± 0.34

Physical lap shear tests for the aluminium- and composite-based SLJs were performed. The aluminium one was tested using an Instron 5500R machine with a 30 kN load cell, wedge-action grips and a displacement rate of 1.0 mm/min at the room temperature, as shown in Fig. 4(a). A mechanical extensometer was mounted at a defined distance of 12.5 mm to measure the relative displacement to the bonded overlapping area of the joint. The experiment for composite one was executed using an Instron 5,800R machine with a 50.0 kN load cell. A video extensometer was used to measure the relative displacement between the two dots at a distance of 10 mm to the adhesive overlap, as shown in Fig. 4(b). All the specimens were loaded under the displacement control. The load and crosshead displacement were re-set to the zero position after a small pre-loading. The aluminium joint was in adhesive failure, and most of the adhesives were left at one side of the adherend, as shown in Fig. 4(c). The composite joint was in cohesive failure, and a thin layer of adhesive was left on both side of the adherends, as shown in Fig. 4(d). It showed that the composite joint was bonded in a comparably better quality as the joint failed within the adhesive, whereas the quality of the aluminium joint could be improved by comparing Fig. 4(c) and Fig. 4(d).

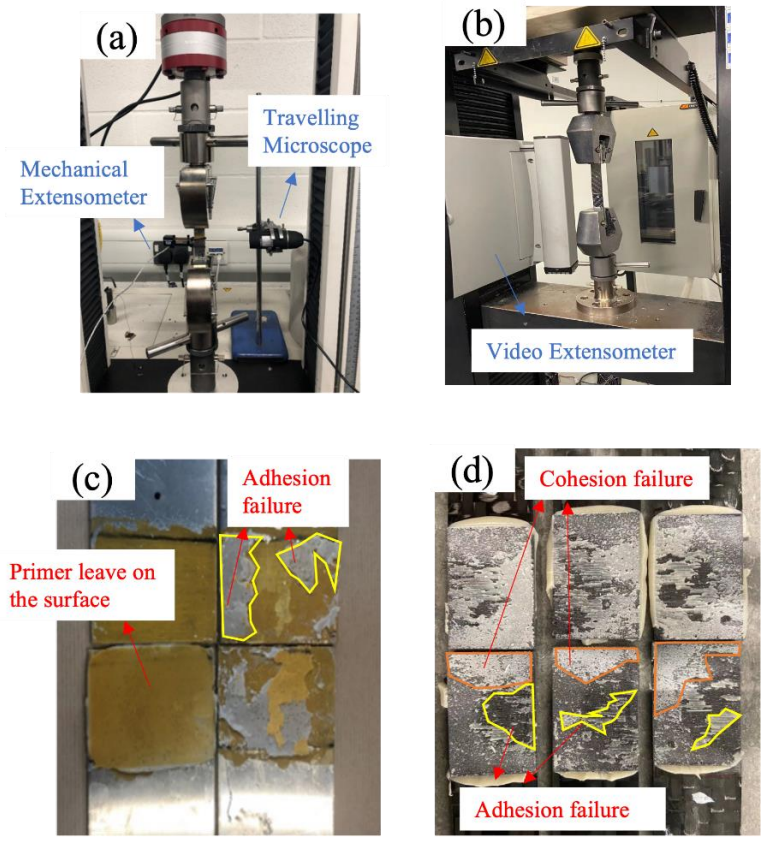

Fig. 4: (a) The setup of a test machine for the aluminium-based SLJs with a mechanical extensometer; (b) The test setup of the composite SLJs with a video extensometer; (c) The failure surfaces of the aluminium SLJs; (d) The failure surfaces of the composite SLJs.

3.3 FEA modelling

Based on the Cohesive Zone Method (CZM), a 2D FEA model was built using the Abaqus software to simulate the failure load of the aluminium and composite SLJs. Apart from constant inputs (material properties) to the FEA model, variable inputs to the FEA model are E_1, E_2, G_1, G_2, and the output of the FEA model is the joint failure load. In this research, the purpose of the FEA model is to generate training samples for the DNN model, which process is depicted in Section 3.4.

In the FEA model, four-noded plane strain elements and cohesive elements were employed to model adherends and adhesive, respectively. The displacements and rotations of the entire nodes at one end were restrained on all the directions, whereas those at the other ends were fixed in the z-direction displacement and rotation. A displacement was applied to the joint till final failure occurred. A mesh size of 0.2 mm was designed at the bonded area after a mesh convergence study, and a gradual mesh size was used for the adherends to save the computational time. The setup of the entire model is shown in Fig. 5. The non-linear geometrical analysis using an explicit solver was taken for a large deformation.

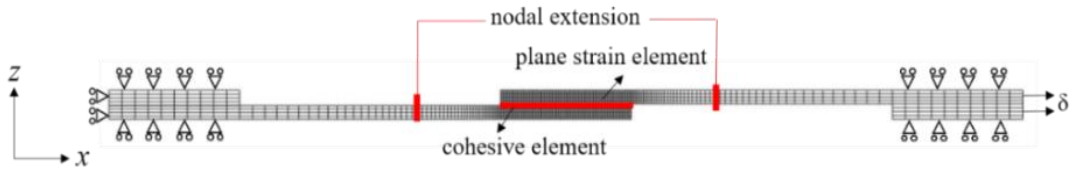

Fig. 5: The loading and boundary conditions of the cohesive zone model.

To ensure the validation of the FEA model, the nodal displacements corresponding to the locations of extensometers were extracted. The joint failure load and its slope against the displacement curve within the linear region of joints were calculated for both experimental and FEA results based on the following Equations (1) and (2). The reason to choose the linear region is that it indicates the stiffness of a joint, which is a key design factor to evaluate the joint's

capability. When an applied load exceeds the linear region, adherend and adhesive materials will rapidly deform plastically and a permanent damage is generated.

$$Load_f(matl, i) = max(F, i) \quad (1)$$

where $Load_f(matl, i)$ represents the failure load of a joint in a specific adherend material (*matl*) for the i^{th} sample (a sample of a joint means a different set of joint parameters used); *F* denotes the load matrix in the experiment or the FEA-based simulation.

The load difference between experimental and FEA results ($\emptyset_1$) is calculated below:

$$\emptyset_1 = \frac{|Load_f(matl,i)\_exp - Load_f(matl,i)\_FEA|}{Load_f(matl,i)\_exp} \times 100 \quad (2)$$

where $Load_f(matl, i)\_exp$ and $Load_f(matl, i)\_FEA$ are joint failure loads obtained based on an experiment and a FEA simulation for the *i-th* sample, respectively.

The FEA model is valid when $\emptyset_1$ is smaller than a pre-defined threshold value. After validation, FEA simulations will be conducted using different joint parameters to produce a training database for the DNN model. The elastic modulus of the materials used for adherends and adhesives has a significant effect on joint performance (Campilho et al., 2012; Campilho et al., 2013). As the cohesive zone model is developed for modelling adhesives, fracture toughness (cohesive energy) in tension and shear are the most critical parameters compared to other cohesive parameters.

The upper and lower ranges of the elastic modulus of upper and lower adherends (E_1 and E_2) were from 60.0 GPa to 200.0 GPa with 4 intervals in a 35.0 GPa gap each (i.e., 60.0, 95.0, 130.0, 165.0, 200.0 GPa). The ranges covered most of the materials, including aluminium, composite and steel. The range of the fracture toughness (G_1) in tension covers from 0.2 N/mm to 1.6 N/mm with 4 intervals in a 0.35 N/mm gap each (i.e., 0.2, 0.55, 0.9, 1.25, 1.6 N/mm). The fracture toughness in shear (G_2) covered from 0.4 to 8.0 N/mm with 4 intervals in a 1.9 N/mm gap each (i.e., 0.4, 2.3, 4.2, 6.1, 8.0 N/mm). The four joint parameters and their values are summarised in Table 2. With the combinations of joint parameter values, a total of 625 samples for a joint were generated.

Table 2: Value settings for the four essential joint parameters.

Parameter (unit)/No. of values	1	2	3	4	5
Parameter a: E_1 (GPa)	60.0	95.0	130.0	165.0	200.0
Parameter b: E_2 (GPa)	60.0	95.0	130.0	165.0	200.0
Parameter c: G_1 (N/mm)	0.2	0.55	0.9	1.25	1.6
Parameter d: G_2 (N/mm)	0.4	2.3	4.2	6.1	8.0

3.4 The improved DNN modelling

3.4.1 The structure of the model

To mine the underlying relationship between joint parameters and the joint failure load, an improved DNN model is designed. A classic DNN model exhibits the following features (Li et al., 2021): (i) It has an ability to represent highly complex and non-linear relationships between input and output; (ii) It does not require much prior physical knowledge regarding adhesively bonded joints, which might be necessary for many other analytical methods; (iii) It can be updated incrementally when new training samples are generated.

In this research, based on the classic DNN model, an improved DNN model with an embedded TL mechanism is designed for joint predictions. Fig. 6 illustrates the structure of the improved DNN model, including fully connected layers, a dropout layer, a batch normalisation layer, a ReLU layer and a TL layer. The input for the improved DNN model is a set of key joint parameters represented as a vector $X = [E_1, E_2, G_1, G_2]$, and the output is the predicted joint failure load based on the joint parameters. The key parameters of the DNN model and the chosen values in this research are shown in Table 3. In the table, the dropout probability was set to 0.2 as instructed in previous research (Hinton et al., 2012). The learning rate of the optimiser was selected from the allowable range of the parameter, which is usually within 0.01-0.1. Trials showed that 0.05 was the appropriate value of the learning rate for this research.

The TL mechanism was implemented after each block of the DNN model. The design was adopted from the authors' previous research (Li et al., 2021). Different structures of the improved DNN model were benchmarked to justify the model design in Section 4.2.

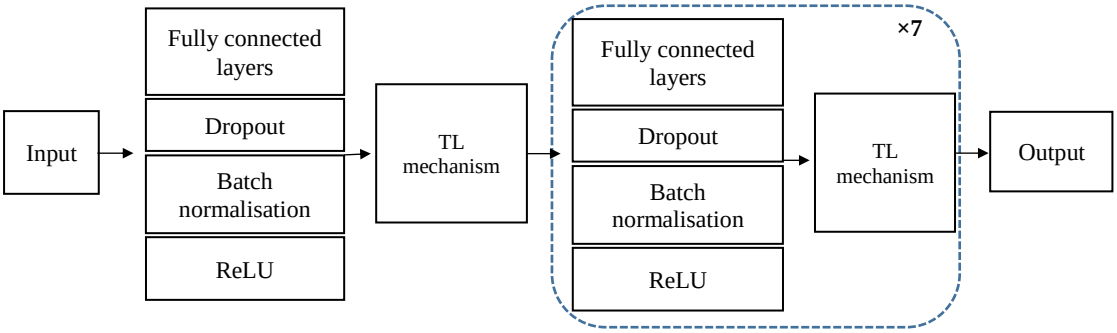

Fig. 6: The structure of the improved DNN model.

Table 3: Key parameters of the improved DNN model.

Functions	Dropout probability	Number of the hidden layers	Number of the hidden neurons	Optimiser	Learning rate
Parameter's value or choice	0.2	8	10	Gradient descent	0.05

3.4.2 Transfer learning

Joint specimens using the same type of adherend materials show a similar trend in displacement against load. As shown in Fig. 7, all aluminium specimens had relatively similar slope ranges (74,784.87N/mm-88,519.93N/mm) and failure load ranges (20,191.91N-20,907.69N) against displacement. All composite specimens also had the similar slope ranges (29,591.29N/mm-39,147.06N/mm) and failure load ranges (8,973.76N-9,307.09N) against displacement. In the meantime, the trends of the joint specimens using dissimilar adherend materials were significantly different. To predict joint failure loads accurately, a normal practice is that a set of new physical tests are conducted, an FEA model is developed and calibrated to enrich the training samples, and the DNN model is re-trained based on the physical tests and FEA simulations. Obviously, it is not an economic process, and the advantage of using the DNN model to perform efficient prediction on joint failure loads is compromised.

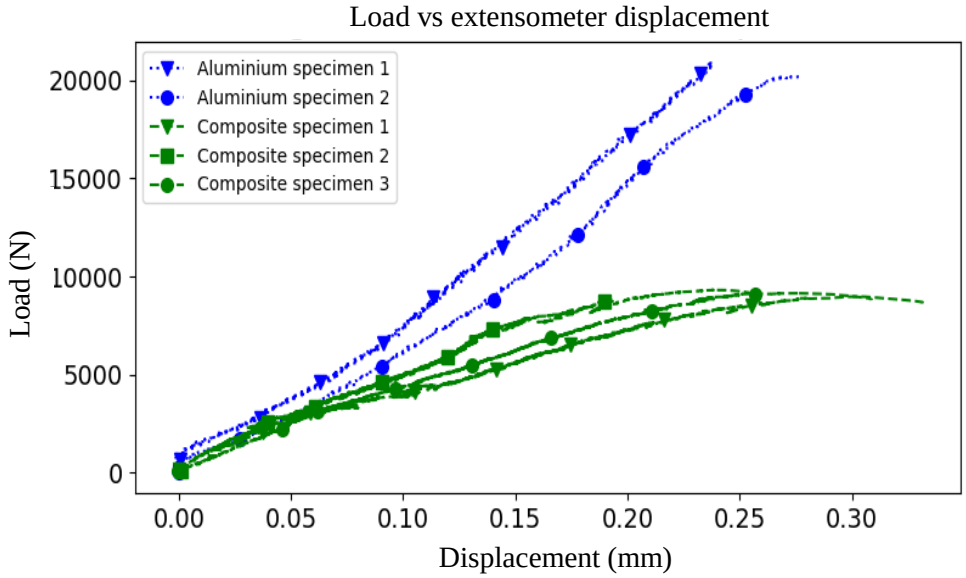

Fig. 7: Displacement vs loads for the aluminium and composite SLJs.

TL is an effective intelligent mechanism to enhance the adaptability of a deep learning model pre-trained for a task (denoted as a source domain) to support a new task (denoted as a target domain) in an efficient and cost-effective means (Zhu et al., 2021). Knowledge is transferred on the basis of resolving the dissimilarities of features and their distributions across different domains, and collected data from a source domain can be re-used in a target domain. In this research, TL is incorporated into the DNN model to alleviate the re-training requirement for the model on a new joint design. To be more specific, based on TL, only a small number of new experimental and FEA simulations for the composite SLJs (the target domain) need to be generated, and the training samples previously collected from the aluminium SLJs (the source domain) can be re-used to support the prediction of the failure loads of the composite SLJs. The process of the TL mechanism is illustrated in Fig 8.

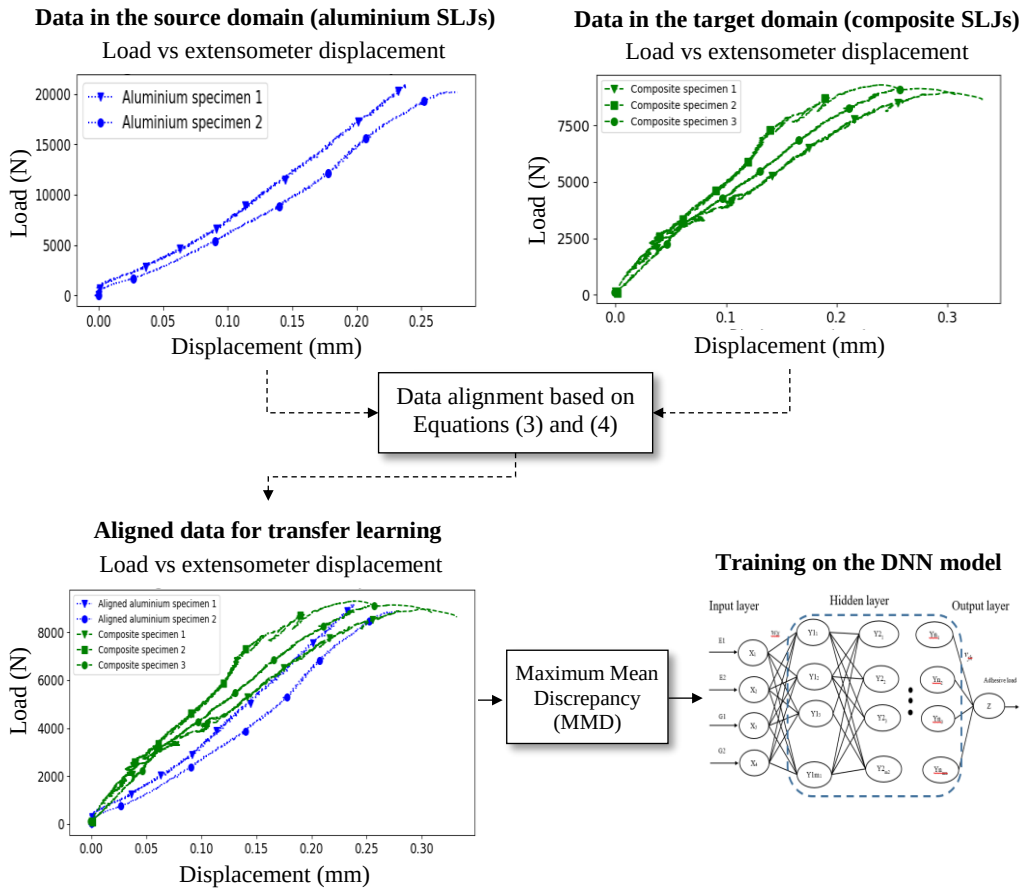

Fig. 8: The transfer learning (TL) process.

To elaborate the TL mechanism in the improved DNN model, some representations are defined. For the aluminium and composite SLJs, assume there are *n* samples each. Each sample, denoted as the i^{th} sample, comprises a set of joint parameters (E_1, E_2, G_1, G_2), and the corresponding joint failure load ($Load_f(Al,i)$ or $Load_f(Compos,i)$). $D_{source} = \{ Load_f(Al,i) , P(Load_f(Al,i)) \}$ represents the source domain, where $P(Load_f(Al,i))$ is the distribution probability of the sample in the source domain. $D_{target} = \{ Load_f(Compos,i) , P(Load_f(Compos,i)) \}$ represents the target domain, where $P(Load_f(Compos,i))$ is the distribution probability of the sample in the target domain. The distribution categories of the 375 samples (selected from 625 samples to optimise the computational time) for the aluminium SLJs are presented in Table 4, where the parameter symbols (a, b, c, d for E_1, E_2, G_1, G_2) and the No. of values (1, 2, 3, 4, 5) are shown in Table 2.

The distribution of data samples is significant to the training accuracy of the DNN model. For instance, if the data samples are mostly located within a certain range (i.e., most data are distributed within the distribution categories from 1 to 8 only), the training accuracy will be compromised as there is no interpolation from other ranges. Therefore, the 30 data samples were randomly selected from all the distribution categories. In this research, the distribution categories were designed to ensure data samples were evenly distributed within the range of the parameters. Fifteen categories were designed as there were 30 data samples in the target domain, so there was at least one data sample from each category to ensure the training accuracy of the DNN model. Critical steps for the TL mechanism in this research are elaborated below.

Table 4: Distributions of the 375 samples of the aluminium SLJ (the source domain).

	a1b1	a1b2	a1b3	a1b4	a1b5	a2b1	a2b2	a2b3	a2b4	a2b5	a3b1	a3b2	a3b3	a3b4	a3b5
c1d1, c1d2 c1d3, c1d4 c1d5	Distribution category 1					Distribution category 6					Distribution category 11				
c2d1, c2d2 c2d3, c2d4 c2d5	Distribution category 2					Distribution category 7					Distribution category 12				
c3d1, c3d2 c3d3, c3d4 c3d5	Distribution category 3					Distribution category 8					Distribution category 13				
c4d1, c4d2 c4d3, c4d4 c4d5	Distribution category 4					Distribution category 9					Distribution category 14				
c5d1, c5d2 c5d3, c5d4 c5d5	Distribution category 5					Distribution category 10					Distribution category 15				

(1) Data alignment between domains

To ensure the effectiveness of the TL mechanism across domains, alignment of the failure loads between the aluminium and composite SLJs is essential (the data alignment process is explained in Fig. 8). The difference between the maximum failure loads of the aluminium and composite SLJs was calculated and minimised based on Equations (3) and (4), respectively. In this research, 30 samples of the composite SLJ were generated using FEA. The selected joint parameters for the composite SLJ are shown in Table 5.

Table 5: Distributions of the samples of the composite SLJ (the target domain).

Distribution category 1	Distribution category 2	Distribution category 3	Distribution category 4	Distribution category 5
a1b5c1d1, a1b3c1d3, a1b5c1d5	a2b2c2d2, a1b5c2d5	a1b5c3d5	a2b2c4d2, a1b5c4d5	a1b3c5d2, a1b5c5d5
Distribution category 6	Distribution category 7	Distribution category 8	Distribution category 9	Distribution category 10
a2b5c1d1, a2b5c1d5	a2b5c2d5, a2b3c2d4	a3b2c3d2, a2b5c3d5	a2b5c4d5, a2b5c4d4	a3b2c5d3, a2b5c5d5

Distribution category 11	Distribution category 12	Distribution category 13	Distribution category 14	Distribution category 15
a3b5c1d1, a3b5c1d5	a3b4c2d2, a3b5c2d5	a3b4c3d4, a3b5c3d5	a3b1c4d3, a3b5c4d5	a3b4c5d1, a3b5c5d5

The difference of samples between two domains (i.e., the aluminium and composite SLJs) can be calculated as follows:

$$\emptyset_2 = \frac{\sum_{i=1}^{30}\left|Load_f(Al,i) - Load_f(Compos,i)\right|}{Load_f(Al,i)} \quad (3)$$

To minimise the overall difference, the failure load of the aluminium SLJ is aligned to that of the composite SLJ as follows:

$$Load_f(Al,i)^* = Load_f(Al,i) \cdot (1 + \emptyset_2) \quad (4)$$

where $Load_f(al,i)^*$ is the aligned failure load of the aluminium joint.

The aligned 375 data samples from the source domain will be combined with the 30 samples in the target domain to train the DNN model (which means that 405 samples were collected for the composite joint for the DNN training, and the data collection time was significantly reduced by 88.63% (i.e., (405-30)/405) in comparison to the solution of generating all the data using FEA).

(2) Maximum Mean Discrepancy (MMD)

MMD was popularly used to measure the distance metric for distribution probabilities between two domains to ensure the effectiveness of TL. The MMDs of the source and target domains are defined below:

$$Mean_H\left(Load_f(Al,i)^*\right) = \frac{1}{m}\sum_{i=1}^{m} H\left(Load_f(Al,i)^*\right) \quad (5)$$

$$Mean_H\left(Load_f(Compos,i)\right) = \frac{1}{m}\sum_{i=1}^{m} H(Load_f(Compos,i)) \quad (6)$$

$$MMD_H\left(Load_f(Al,i)^*, Load_f(Compos,i)\right) = sup(Mean_H\left(Load_f(Al,i)^*\right) - Mean_H\left(Load_f(compos,i)\right)) \quad (7)$$

where $sup(\cdot)$ is the supremum of the aggregate; $H(\cdot)$ is a RKHS (Reproducing Kernel Hilbert Space).

Calculated MMD is used as part of the loss function to re-train the DNN model. The loss function ($\emptyset_3$) is calculated based on MMD and Mean Squared Error (MSE) below:

$$MSE = \frac{\sum_{i=1}^{n}(z_i - yz_i)^2}{n} \quad (8)$$

where n is the total results of the of the DNN model (n=1 in this case as there is only 1 output); z_i is the *i-th* ground-truth and yz_i is the *i-th* predicted output.

$$\emptyset_3 = w_1 \cdot MMD_H\left(Load_f(Al,i)^*, Load_f(Compos,i)\right) + w_2 \cdot MSE \quad (9)$$

where w_1 and w_2 are the weights. MSE is calculated according to Equation (8). The DNN model is trained by minimising the loss function using the gradient descent optimiser (Zhao et al., 2021). In this study MMD and MSE are equally important to ensure the training accuracy of the DNN model, so that $w_1 = w_2 = 0.5$.

3.5 Fruit fly optimisation

Based on the prediction results from the improved DNN model, a designed FFO algorithm can be conducted to search for optimal joint parameters (E_1, E_2, G_1, G_2) iteratively to identify the maximised value of the joint failure load. The FFO algorithm is a relatively new swarm algorithm being capable of providing multiple swarm groups around each swarm centre to implement parallel search. The algorithm imitates the behaviours of fruit flies according to the following two steps: (i) Smell-based search: fruit flies are randomly generated around each swarm centre, and the smell concentration (fitness) of each fruit fly is calculated. The optimal solution is usually unknown due to its non-linearity characteristics, so that local optimal solutions can be avoided (Qin et al., 2022); (ii) Vision-based search: the fruit fly with the best fitness in each swarm centre replaces the original swarm centre, through which the best fitness can be maintained while the swarm centres are approaching the best solution efficiently (Ibrahim et al., 2022). In summary, the FFO algorithm is featured with parallel search, local optima avoidance, simple implementation and quick convergence (Liang et al., 2021). Based on benchmarking analyses with several main-stream optimisation algorithms (details are given in Section 4.3), it reveals that the FFO algorithm is suitable for this multi-parameter and non-linear optimisation problem, and easy to be integrated with the DNN model. The process of the FFO algorithm is illustrated in Fig. 9, and the step-wise flow is elaborated in Fig. 10.

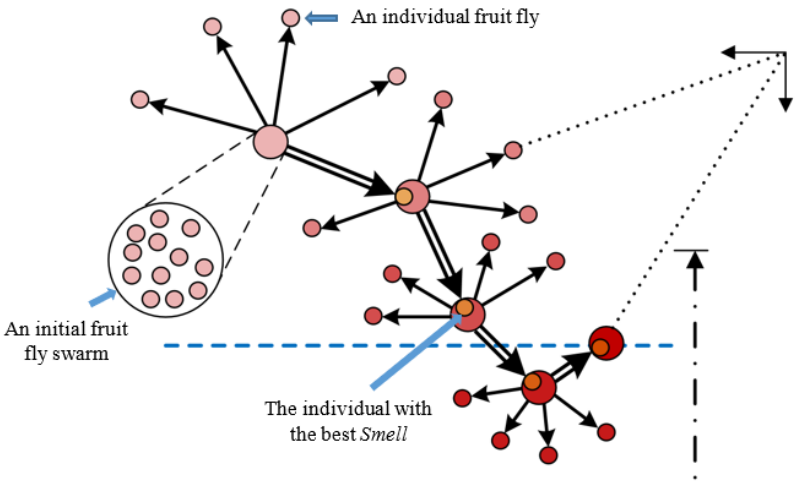

Fig. 9: The illustration of the FFO algorithm.

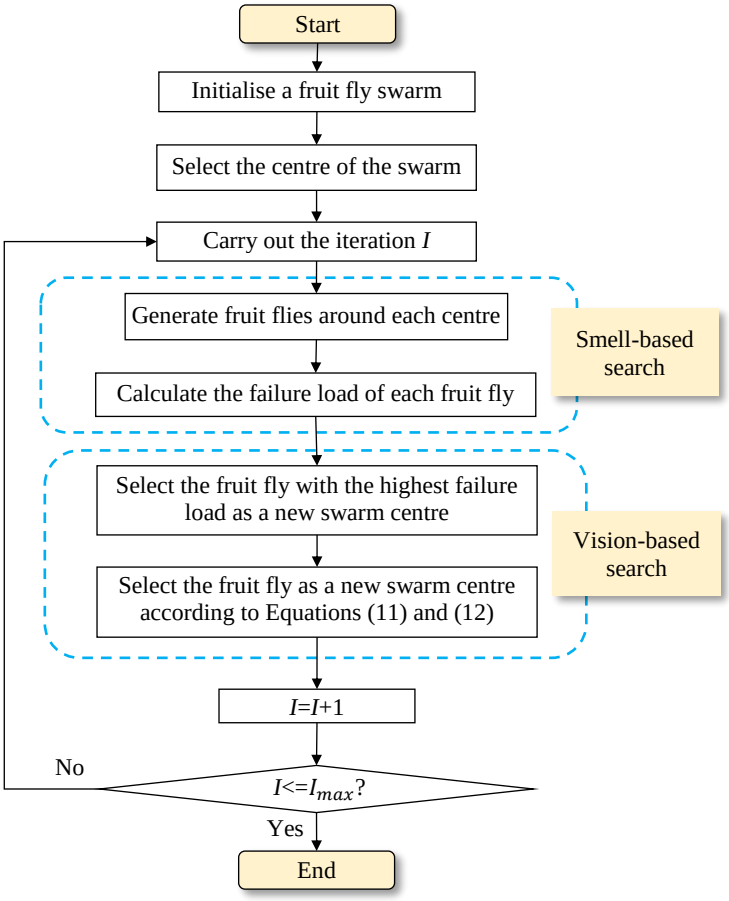

Fig. 10: The flow of the FFO algorithm for the joint parameter optimisation.

The major steps in the FFO algorithm are below:

I. *Initialisation*: An initial fruit fly swarm with n fruit flies (each fruit fly is a joint design) are randomly generated. Each fruit fly is modelled to contain four joint parameters, i.e., E_1, E_2,

G_1, *and* G_2. Random values of the joint parameters within their upper and lower boundaries are assigned to the fruit flies:

$$fly_i = LB_i + (UB_i - LB_i) \times rand() \tag{10}$$

where fly_i $(i = 1, \dots, n)$ is a fruit fly; LB_i and UB_i are the lower and upper boundaries of the joint parameters for the fruit fly, respectively; $rand()$ is a random value between 0 and 1.

II. *Iterations*: The following steps are iteratively conducted until the maximum number of iterations is reached:

(2.1) *Selection of the swarm centre:* For fly_i $(i = 1, \dots, n)$, the trained DNN model is employed to predict the joint failure load of the fruit fly (the joint failure load of the fruit fly is represented as $Load_f(fly_i)$). The fruit fly in the swarm with the maximum failure load is chosen as the swarm centre (fly_{centre});

(2.2) *Smell-based search*: A fruit fly around the swarm centre is generated as a new fruit fly according to the following:

$$new\_fly_i = fly_i \times (1 + a \times (rand() - 0.5)) \tag{11}$$

where new_fly_i is a new fruit fly; $rand()$ is a randomly generated value between 0 and 1 to ensure that randomness is embedded in the search process to avoid local optima; a is the search step (trials show that when a was chosen 0.2 in this case study, the fruit fly approached an optimal solution more efficiently).

(2.3) *Vision-based search*: The joint failure loads of all new fruit flies are predicted by using the trained DNN model. If the joint failure load of a fruit fly, denoted as new_fly_k, is greater than that of the original swarm centre, this fruit fly will be used to replace the original swarm centre. However, there is a possibility of accepting the new fruit fly even with a lower value of the joint failure load in order to avoid local optima when the following conditions are satisfied:

$$c > rand() \tag{12}$$

$$c = exp(-\left|Load_f(new\_fly_k) - Load_f(fly_{centre})\right|/I) \tag{13}$$

where c is the value to determine whether the swarm centre with a worse joint failure load will be accepted or not; I is the current iteration.

(2.4)The smell-based search and vision-based search are iterated until reaching the maximum iteration I_{max}.

4. Case Studies and Analyses

4.1 Experiments and FEA-based simulation

To validate the FEA model, experimental and FEA results for the load vs. extensometer displacement relations are demonstrated in Fig. 11. According to Equation (2), the difference between an experimental result and a FEA result ($\emptyset_1$) was calculated and summarised in Table 6. It shows that the locations of the reflecting pads by the FEA model correlate to that of the experiments well.

Table 6: Difference between the experimental and FEA results.

Aluminium	**Specimen 1**	**Specimen 2**		**FEA**
Failure load (N)	20,907.69	20,191.91		21,432.25
Failure load difference ($\emptyset_1$)	2.51%	6.14%		
Composite	**Specimen 1**	**Specimen 2**	**Specimen 3**	**FEA**
Failure load (N)	8,973.76	9,307.09	9,146.83	9,408.82
Failure load difference ($\emptyset_1$)	4.85%	1.09%	2.86%	

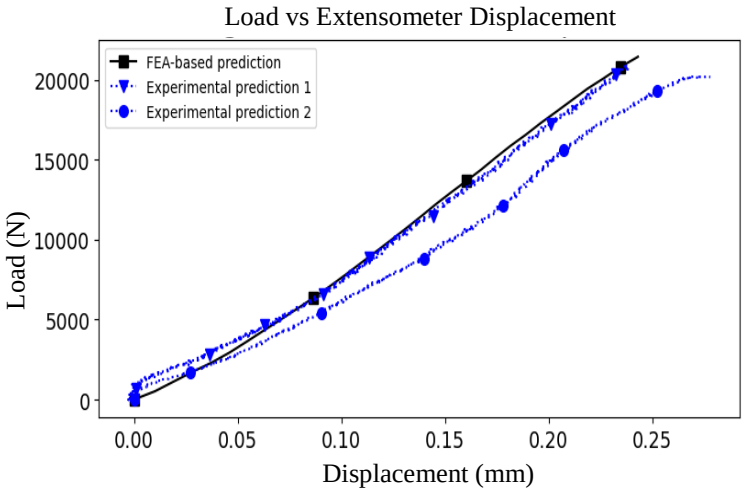

(a) Comparisons of the load vs extensometer displacement relations from experimental results and FEA-based prediction for the aluminium SLJs.

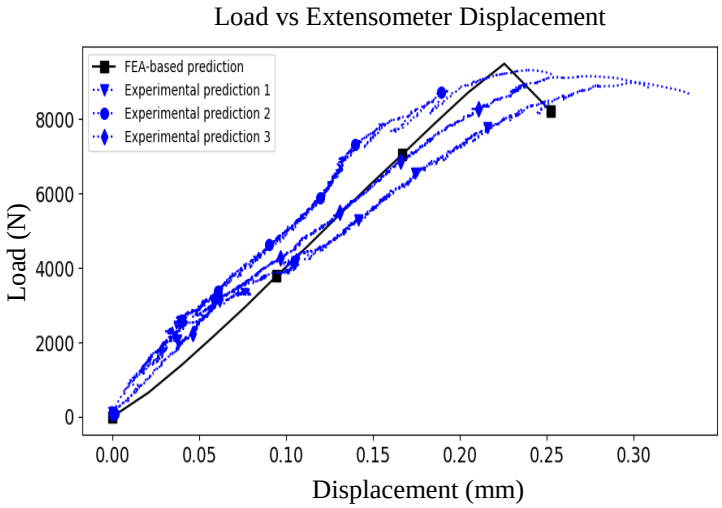

(b) Comparison of load vs extensometer displacement relations from experimental results and FEA-based prediction for the composite SLJs.

Fig. 11: Comparisons of the load vs. extensometer displacement relations.

4.2 The improved DNN model

Datasets generated from the FEA model were used to train the DNN model. Considering the heavy computational load of the FEA model, it is essential to minimise the number of datasets generated from the FEA model as long as the trained DNN model is satisfactory. That is, it is expected to achieve a trade-off between the training accuracy of the DNN model and the computational time of the FEA model. To achieve the balance, the following evaluation and performance criteria are defined:

(i) The training accuracy of the DNN model is evaluated by the loss function ($\emptyset_4$):

$$\emptyset_4(i) = Load_f(matl,i)\_DNN - Load_f(matl,i)\_FEA \quad (14)$$

where $Load_f(matl,i)\_FEA$ is the ground-truth value by the FEA model, and $Load_f(matl,i)\_DNN$ is the predicted joint failure load by the DNN model for the i^{th} dataset.

(ii) The normalised accuracy of the trained DNN model and the normalised computational time required for the FEA model to generate the training samples are defined below:

$$N(\emptyset_4(i)) = \frac{MSE(i) - Min(MSE)}{Max(MSE) - Min(MSE)} \quad (15)$$

$$N(FEA\_time(i)) = \frac{FEA\_time(i) - Min(FEA\_time)}{Max(FEA\_time) - Min(FEA\_time)} \quad (16)$$

where $N(\emptyset_4(i))$ and $N(FEA\_time(i))$ are the normalised training accuracy and the normalised computational time.

(iii) The prediction performance indicator is defined below:

$$P = (v_1 \cdot N(\emptyset_4(i)) + v_2 \cdot N(FEA\_time(i)) \quad (17)$$

where P is the prediction performance; v_1 and v_2 are weights ($v_1 + v_2 = 1$).

The optimal number of training samples generated from the FEA model was determined when the smallest P was achieved. In this research, the prediction accuracy is more important than the computational time, so that v_1 and v_2 were set 0.9 and 0.1, respectively. Fig. 12(a) shows that the normalised prediction accuracy and computational efficiency under different numbers of training samples generated by the FEA model (the number of the datasets range was set from 100 samples to 375 samples in this case study). Fig. 12(b) shows the overall performance under different numbers of training samples by FEA. It indicates that the best value of performance (P) was 0.0853 when the number of the training samples was 264.

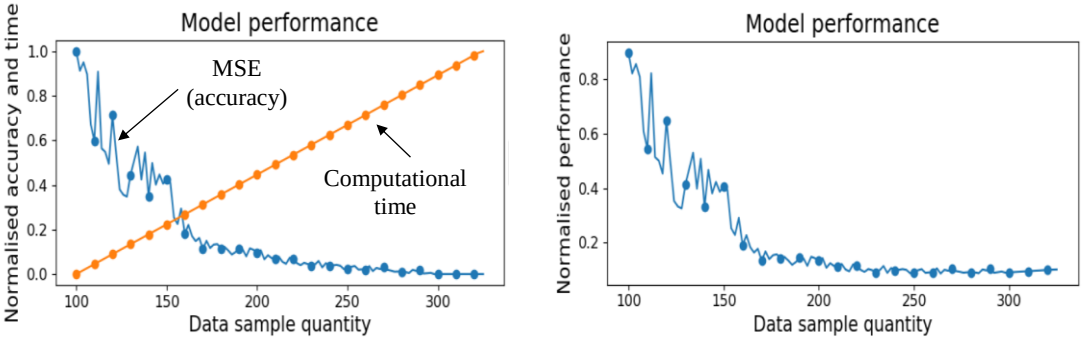

(a) The normalised prediction accuracy and computational time under different numbers of FEA-generated training samples.

(b) The model performance (*P*) under different numbers of FEA-based generated training samples.

Fig. 12: The model performance under different numbers of FEA-based training samples.

To ensure the best structure of the DNN model, different structures were benchmarked over 10 simulations, and the average result was generated. Some results are shown in Table 7 (with 264 FEA-generated datasets for the aluminium SLJ). It indicates that, under 150 training epochs, the structure of the DNN model with 8 hidden layers and 10 nodes in each hidden layer exhibited the best average training accuracy and the second-best average test accuracy, and the training/prediction time is in the same scale in comparison with those of other structures. Thus, the structure of 8 hidden layers and 10 nodes in each hidden layer was used in the design of the DNN model.

Table 7: The training accuracies with different structures of the DNN model.

	Average training accuracy	Average test accuracy	Worst training accuracy	Training time (s)	Prediction time (s)
8 hidden layers, 10 nodes	**0.0611**	**0.0741**	**0.0761**	**5.57**	**1.29**
8 hidden layers, 8 nodes	0.0863	0.0107	0.0995	5.23	1.20
8 hidden layers, 12 nodes	0.0751	0.0931	0.0931	5.91	1.32
6 hidden layers, 10 nodes	0.0921	0.1121	0.1040	5.11	1.19
7 hidden layers, 10 nodes	0.0699	0.0883	0.0810	5.46	1.22
9 hidden layers, 10 nodes	0.0677	0.0771	0.0868	5.61	1.30
10 hidden layers, 10 nodes	0.0651	0.0798	0.0775	5.90	1.51

To train the DNN model to support the composite SLJs, a small number of training samples need to be collected to support the application of the TL mechanism. In this case study, 30 data samples of the composite joint were collected. MMD was used to reduce the distribution difference in the datasets between the source domain (the aluminium SLJs) and the target domain (the composite SLJs). To justify the advantage of the TL mechanism, benchmarks were conducted and the results are illustrated in Fig. 13 and Table 8. It showed that the TL mechanism with sample alignment and MMD achieved the best MSE (0.0738).

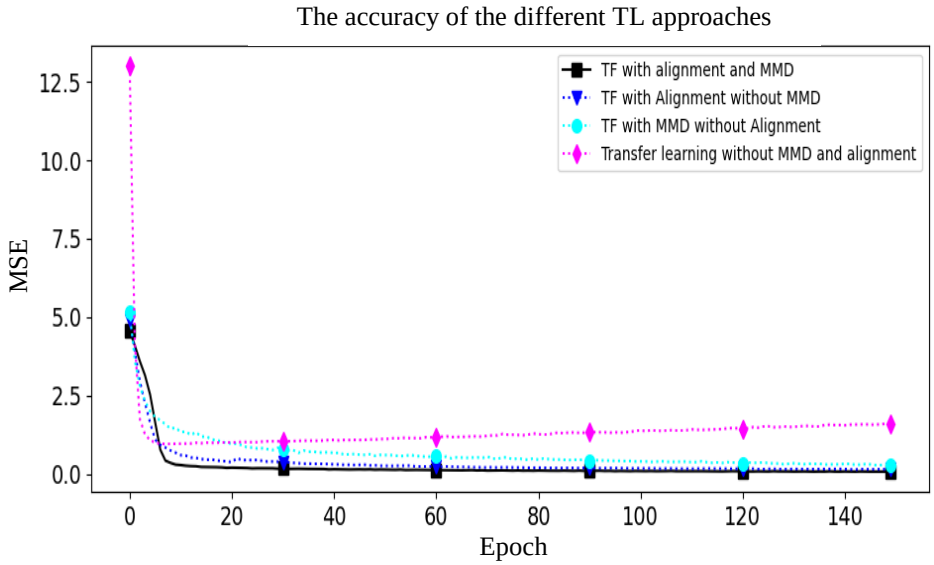

Fig. 13: Benchmark for different transfer learning approaches.

Table 8: Benchmark for the TL mechanisms with different settings.

	Average training accuracy	Average testing accuracy	Worst training accuracy
With alignment and MMD	0.0558	0.0738	0.0869
With alignment but without MMD	0.1277	0.1475	0.1663
With MMD but without alignment	0.2514	0.2799	0.2911
Without alignment and MMD	1.5966	1.6110	1.9421

4.3 The FFO algorithm

The time complexities of the FFO algorithm and the DNN model can be analysed using the following equation:

$$TX_1 = \mathrm{O}(n \times M \times P \times N \times \mathrm{e}) \tag{18}$$

where TX_1 is the time complexity of the DNN model; n is number of input variables ($n = 4$); M is number of hidden neurons ($M = 10$); P is number of the output parameters (P=1 as it predicts only maximum failure load); N is number of observations (indicating the data sample size and it is 264 in this case); e is the number of iterative epochs ($e = 150$) (Fei et al., 2019).

$$TX_2 = O(n_g \times n_0 \times {n_p}^3) \tag{19}$$

where TX_2 is the time complexity of the FFO algorithm; n_g is the number of the iterations in the algorithm ($n_g = 50$); n_0 is the number of optimisation objectives ($n_0 = 1$); n_p is the population size ($n_p = 5$) (Liang et al., 2019).

$TX_1 = O(1584000)$ and $TX_2 = (1250)$, which indicates that the DNN model and the FFO algorithm have relatively low time complexity. Therefore, the approach has good computational efficiencies in optimising joint parameters for failure load enhancement.

To further showcase the optimisation efficiency and robustness of the FFO algorithm, different optimisation algorithms, including PSO, NSGA-II, GA and SA, were compared. Each algorithm was executed 30 times, and the average results were taken. For the FFO algorithm, it took 9 iterations to achieve optimal results. It was quicker than the convergence time for all the other algorithms. All the optimisation algorithms reached the same optimised result, i.e., 18910.57 N. E_1, E_2, G_1 and G_2 were set as 200.0 (GPa), 200.0 (GPa), 1.6 (N/mm) and 8.0 (N/mm), respectively.

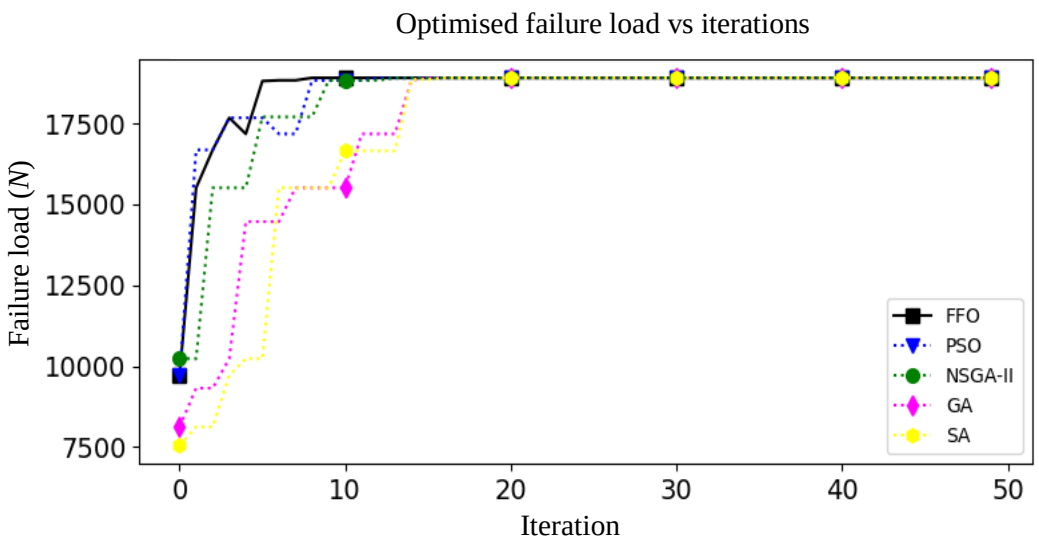

Fig. 14: Benchmark of different optimisation approaches.

Table 9: Optimisation results compared with different optimisation algorithms.

	FFO	PSO	NSGA-II	GA	SA
Iterations to achieve optimal results	9	13	14	15	17
Optimised results (*N*)	18,910.57	18,910.57	18,910.57	18,910.57	18,910.57
Error in the failure load predictions (%)	6.35%	6.35%	6.35%	6.35%	6.35%

4.4 Result discussions and future work

In this research, the focus was on the investigation of designing an innovative deep learning model enabled by a TL mechanism to realise an adaptive prediction on a new joint design using a smaller set of training samples. SLJ designs were used to exemplify and validate the approach. Tests for the adherend and adhesive were designed based on standards. That is, G1 and G2 are mode I and mode II fracture toughness of an adhesive. The two parameters were measured by the mode I double cantilever beam (DCB) and the mode II end notch flexure (ENF) standard tests according to the ISO 15024 standard (2001) and ASTM D6671 (2006). Nevertheless, there are still some limits to the research, and the following aspects should be investigated:

More complex geometrical features (e.g., adhesive length and thickness) have significant effects on joints' lap shear strength (Banea and da Silva, 2009; Budhe et al., 2017). In the future, geometrical features, together with key process parameters, will be investigated to improve joint designs.

Furthermore, investigations will be carried out to understand how other joint parameters, such as the treatment parameters, the bonding type, and the density of fibres, generate impacts on joint failure loads. Based on the investigations, a more comprehensive DNN model to evaluate and predict the joint failure load could be developed.

In the research, case studies were based on the same E (E_1=E_2). The approach is applicable to hybrid joint designs using different E_1 and E_2. Further investigation on joint designs with different E values will be carried out in the future.

5. Conclusions

The failure load of an adhesively bonded joint is one of the most influential factors in determining the integrity and bonding performance of the joint. To address this issue, this paper presents a novel improved DNN model and FFO algorithm-enabled approach to predict joint failure loads and optimise the joint design based on the prediction results efficiently. The innovations of this research can be summarised below:

- A TL mechanism is incorporated into the DNN model to carry out efficient predictions on new joint designs by adapting the pre-trained DNN model. Case studies showed that the number of datasets and the computational time (compared with the FEA model) required to re-train the DNN model for a new SLJ design were reduced by 92.00% (i.e., (375-30)/375)) and 99.57% (i.e., (1186.04s-5.1s)/1186.04s), respectively. It clearly evinces the effectiveness of the approach in terms of computational efficiency improvement and training sample reduction;
- An FFO algorithm is augmented with the DNN model to fine-tune joint parameters to attain design optimisation based on iterative predictions on the joint failure load. A good optimisation efficiency is achieved by leveraging the parallel computing feature embedded in the FFO algorithm and the TL mechanism-driven predictions. Experiments proved that the approach reached optimal results much more quickly (only within 9 iterations) in comparison with several other mainstream optimisation algorithms. The experiments also revealed that the failure load of a new SLJ design was substantially increased by 9.96% (i.e., (18910.57N-17197.68N)/17197.68N).

Acknowledgement:

This research was funded by the National Natural Science Foundation of China (Project No. 51975444), and partially funded by the UK industrial and research partners (the Unipart Powertrain Application Ltd. (UK) and the Institute of Digital Engineering (UK)).

Conflicts of Interest:

The authors declare no conflict of interest. The funders had no role in the design of the study; in the collection, analyses, or interpretation of data; in the writing of the manuscript, or in the decision to publish the results.

References:

Abdel-Monsef, S., Renart, J., Carreras, L., Turon, A., & Maimí, P. (2021). Effect of environment conditioning on mode II fracture behaviour of adhesively bonded joints. Theoretical and Applied Fracture Mechanics, 112, p. 102912. doi: 10.1016/j.tafmec.2021.102912.

Akpinar, S., & Sahin, R. (2021). The fracture load analysis of different material thickness in adhesively bonded joints subjected to fully reversed bending fatigue load. Theoretical and Applied Fracture Mechanics, 114, p. 102984. doi: 10.1016/j.tafmec.2021.102984.

Arhore, E., Yasaee, M. and Dayyani, I. (2021). Comparison of GA and topology optimization of adherend for adhesively bonded metal composite joints. International Journal of Solids and Structures, 226-227, p.111078.

ASTM D3165 (2014). Strength properties of adhesives in shear by tension loading of single-lap-joint laminated assemblies. 07.

Atta, M., Abd-Elhady, A., Abu-Sinna, A., & Sallam, H. (2019). Prediction of failure stages for double lap joints using finite element analysis and artificial neural networks. Engineering Failure Analysis, 97, pp. 242-257. doi: 10.1016/j.engfailanal.2019.01.042.

Banea, M.D., & da Silva, L.F.M. (2009), Adhesively bonded joints in composite materials: An overview, Proceedings of the Institution of Mechanical Engineers, Part L: Journal of Materials: Design and Applications, 223, 1, pp. 1–18. doi.org/10.1243/14644207JMDA219.

Barzegar, M., Pasadas, D., Ribeiro, A. and Ramos, H. (2021). Classification Functions and Optimization Algorithms for Debonding Detection in Adhesively Bonded Lap-joints

through Ultrasonic Guided Waves. 2021 IEEE UFFC Latin America Ultrasonics Symposium (LAUS),.

Behera, R., Parida, S., & Das, R. (2020). 3-D interfacial stress analysis of adhesively bonded curved laminated FRP composite single lap joint. Materials Today: Proceedings, 26, pp. 1948-1952. doi: 10.1016/j.matpr.2020.02.426.

Budhe, S., Banea, M.D., de Barros, S., & da Silva, L.F.M. (2017), An updated review of adhesively bonded joints in composite materials, International Journal of Adhesion and Adhesives, 72, pp. 30–42. doi.org/10.1016/j.ijadhadh.2016.10.010.

Campilho, R., Banea, M., Neto, J., & da Silva, L.F.M. (2012). Modelling of single-lap joints using cohesive zone models: Effect of the cohesive parameters on the output of the simulations. The Journal of Adhesion, 88(4-6), pp. 513-533. doi: 10.1080/00218464.2012.660834.

Campilho, R., Banea, M., Neto, J., & da Silva, L.F.M. (2013). Modelling adhesive joints with cohesive zone models: effect of the cohesive law shape of the adhesive layer. International Journal of Adhesion and Adhesives, 44, pp. 48-56. doi: 10.1016/j.ijadhadh.2013.02.006.

Carbas, R., da Silva, L., Madureira, M., & Critchlow, G. (2014). Modelling of functionally graded adhesive joints. The Journal of Adhesion, 90(8), pp. 698-716. doi: 10.1080/00218464.2013.834255.

Dehaghani, R., Cronin, D., & Montesano, J. (2021). Performance and failure assessment of adhesively bonded non-crimp fabric carbon fiber/epoxy composite single lap joints. International Journal of Adhesion and Adhesives, 105, p. 102776. doi: 10.1016/j.ijadhadh.2020.102776.

Demir, K., Bayramoglu, S., & Akpinar, S. (2020). The fracture load analysis of different support patches in adhesively bonded single-lap joints. Theoretical and Applied Fracture Mechanics, 108, p. 102653. doi: 10.1016/j.tafmec.2020.102653.

Djebbar, N., Boutabout, B., Boulenouar Rachid, H. & Oudad, W. (2022). Effect of spew adhesive and beveling substrate geometrical shape on stresses in a bonded single lap joint. Engineering Structures, 256, p.114049. doi: 10.1016/j.engstruct.2022.114049.

Fei, X., Shah, N., Verba, N., Chao, K., Sanchez-Anguix, V., Lewandowski, J., James, A. & Usman, Z. (2019). CPS data streams analytics based on machine learning for cloud and fog computing: A survey. Future Generation Computer Systems, 90, pp. 435-450. doi: 10.1016/j.future.2018.06.042.

Gavgali, E., Sahin, R., & Akpinar, S. (2021). An investigation of the fatigue performance of adhesively bonded step-lap joints: An experimental and numerical analysis. International Journal of Adhesion and Adhesives, 104, p. 102736. doi: 10.1016/j.ijadhadh.2020.102736.

Gu, Z., Liu, Y., Hughes, D., Ye, J., & Hou, X. (2021). A parametric study of adhesive bonded joints with composite material using black-box and grey-box machine learning methods: Deep neuron networks and genetic programming. Composites Part B: Engineering, 217, p. 108894. doi: 10.1016/j.compositesb.2021.108894.

Hinton, G., Srivastava, N., Krizhevsky, A., Sutskever, I., & Salakhutdinov, R. (2012) Improving neural networks by preventing co-adaptation of feature detectors. arXiv:1207.0580v1.

Huntsman (2015). Araldite 2015 Technical Data Sheet. https://krayden.com/technical-data-sheet/huntsman-araldite-2015-tds/ (last accessed on 05.10.2022).

Ibrahim, I., Hossain, M. & Duck, B. (2022). A hybrid wind driven-based fruit fly optimization algorithm for identifying the parameters of a double-diode photovoltaic cell model considering degradation effects. Sustainable Energy Technologies and Assessments, 50, p. 101685. doi: 10.1016/j.seta.2021.101685.

Jairaja R., & Naik, G. (2019). Single and dual adhesive bond strength analysis of single lap joint between dissimilar adherends. International Journal of Adhesion and Adhesives, 92, pp. 142-153. doi: 10.1016/j.ijadhadh.2019.04.016.

Kim, M., Hong, H., & Kim, Y. (2021). Determination of failure envelope of functionally graded adhesive bonded joints by using mixed mode continuum damage model and response surface method. International Journal of Adhesion and Adhesives, 106, p. 102815. doi: 10.1016/j.ijadhadh.2021.102815.

Kupski, J., & Teixeira de Freitas, S. (2021). Design of adhesively bonded lap joints with laminated CFRP adherends: Review, challenges and new opportunities for aerospace structures. Composite Structures, 268, p. 113923. doi: 10.1016/j.compstruct.2021.113923.

Li, W.D., Liang, Y.C., & Wang, S. (2021). Data Driven Smart Manufacturing Technologies and Applications. Springer.

Liang, Y., Li, W.D., Lu, X. & Wang, S. (2019). Fog computing and convolutional neural network enabled prognosis for machining process optimization. Journal of Manufacturing Systems, 52, pp. 32-42. doi: 10.1016/j.jmsy.2017.02.011.

Liang, Y.C., Lu, X., Li, W.D., & Wang, S. (2018). Cyber physical system and big data enabled energy efficient machining optimisation. Journal of Cleaner Production, 187, pp. 46-62. doi: 10.1016/j.jclepro.2018.03.149.

Liu, Y., Gu, Z., Hughes, D., Ye, J., & Hou, X. (2021). Understanding mixed mode ratio of adhesively bonded joints using genetic programming (GP). Composite Structures, 258, p. 113389. doi: 10.1016/j.compstruct.2020.113389.

Mahjoubi, S., Barhemat, R., Guo, P., Meng, W. and Bao, Y. (2021). Prediction and multi-objective optimization of mechanical, economical, and environmental properties for strain-hardening cementitious composites (SHCC) based on automated machine learning and metaheuristic algorithms. Journal of Cleaner Production, 329, p.129665.

Matta, S., & Ramji, M. (2019). Prediction of mechanical behaviour of adhesively bonded CFRP scarf jointed specimen under tensile loading using localised DIC and CZM. International Journal of Adhesion and Adhesives, 89, pp. 88-108. doi: 10.1016/j.ijadhadh.2018.12.002.

Motlagh, S. and Naghizadehrokni, M. (2022). An extended multi-model regression approach for compressive strength prediction and optimization of a concrete mixture. Construction and Building Materials, 327, p.126828.

Ojalvo, I., & Eidinoff, H. (1978). Bond Thickness Effects upon Stresses in Single-Lap Adhesive Joints. AIAA Journal, 16(3), pp. 204-211. doi: 10.2514/3.60878.

Qin, S., Pi, D., Shao, Z. & Xu, Y. (2022). Hybrid collaborative multi-objective fruit fly optimization algorithm for scheduling workflow in cloud environment. Swarm and Evolutionary Computation, 68, p. 101008. doi: 10.1016/j.swevo.2021.101008.

Ramalho, L., Campilho, R., & Belinha, J. (2020a). Single lap joint strength prediction using the radial point interpolation method and the critical longitudinal strain criterion. Engineering Analysis with Boundary Elements, 113, pp. 268-276. doi: 10.1016/j.enganabound.2020.01.010.

Ramalho, L., Campilho, R., Belinha, J., & da Silva, L. (2020b). Static strength prediction of adhesive joints: A review. International Journal of Adhesion and Adhesives, 96, p. 102451. doi: 10.1016/j.ijadhadh.2019.102451.

Sadeghi, M., Gabener, A., Zimmermann, J., Saravana, K., Weiland, J., Reisgen, U., & Schroeder, K. (2020). Failure load prediction of adhesively bonded single lap joints by using various FEM techniques. International Journal of Adhesion and Adhesives, 97, p. 102493. doi: 10.1016/j.ijadhadh.2019.102493.

Shang, X., Marques, E., Machado, J., Carbas, R., Jiang, D., & da Silva, L.F.M. (2019). Review on techniques to improve the strength of adhesive joints with composite adherends. Composites Part B: Engineering, 177, p. 107363. doi: 10.1016/j.compositesb.2019.107363.

Shi, J., Cao, W., & Wu, Z. (2019). Effect of adhesive properties on the bond behaviour of externally bonded FRP-to-concrete joints. Composites Part B: Engineering, 177, p. 107365. doi: 10.1016/j.compositesb.2019.107365.

Stein, N., Mardani, H., & Becker, W. (2016). An efficient analysis model for functionally graded adhesive single lap joints. International Journal of Adhesion and Adhesives, 70, pp. 117-125. doi: 10.1016/j.ijadhadh.2016.06.001.

Stein, N., Weißgraeber, P., & Becker, W. (2016). Stress solution for functionally graded adhesive joints. International Journal of Solids and Structures, 97-98, pp. 300-311. doi: 10.1016/j.ijsolstr.2016.07.019.

Tanaka, H., Mori, Y., Kumekawa, N. and Matsuzaki, R. (2021). Multi-objective optimization of weight and strength of laminated composites using gap-less and overlap-less variable thickness fiber placement. Composite Structures, 276, p.114562.

Wang, B., Xie, L., Song, J., Zhao, B., Li, C., & Zhao, Z. (2021). Curved fatigue crack growth prediction under variable amplitude loading by artificial neural network. International Journal of Fatigue, 142, p. 105886. doi: 10.1016/j.ijfatigue.2020.105886.

Ye, J., Yan, Y., Hong, Y., & Guo, F. (2019). An integrated constitutive model for tensile failure analysis and overlap design of adhesive-bonded composite joints. Composite Structures, 223, p. 110986. doi: 10.1016/j.compstruct.2019.110986.

Zhao, J., Zhang, R., Zhou, Z., Chen, S., Jin, J., & Liu, Q. (2021). A neural architecture search method based on gradient descent for remaining useful life estimation. Neurocomputing, 438, pp. 184-194. doi: 10.1016/j.neucom.2021.01.072.

Zhu, W., Braun, B., Chiang, L., & Romagnoli, J. (2021). Investigation of transfer learning for image classification and impact on training sample size. Chemometrics and Intelligent Laboratory Systems, 211, p. 104269. doi: 10.1016/j.chemolab.2021.104269.